

45. Piva R, Ruggeri B, Williams M, Costa G, Tamagno I, et al. (2008) CEP-18770: A novel, orally active proteasome inhibitor with a tumor-selective pharmacologic profile competitive with bortezomib. *Blood* 111: 2765–2775.
46. Kupperman E, Lee EC, Cao Y, Bannerman B, Fitzgerald M, et al. (2010) Evaluation of the proteasome inhibitor MLN9708 in preclinical models of human cancer. *Cancer Res* 70: 1970–1980.
47. Chauhan D, Singh AV, Aujay M, Kirk CJ, Bandi M, et al. (2010) A novel orally active proteasome inhibitor ONX 0912 triggers in vitro and in vivo cytotoxicity in multiple myeloma. *Blood* 116: 4906–4915.
48. Millward M, Price T, Townsend A, Sweeney C, Spencer A, et al. (2012) Phase 1 clinical trial of the novel proteasome inhibitor marizomib with the histone deacetylase inhibitor vorinostat in patients with melanoma, pancreatic and lung cancer based on in vitro assessments of the combination. *Invest New Drugs* 30: 2303–2317.
49. Moreau P, Richardson PG, Cavo M, Orłowski RZ, San Miguel JF, et al. (2012) Proteasome inhibitors in multiple myeloma: 10 years later. *Blood* 120: 947–959.
50. Chauhan D, Tian Z, Zhou B, Kuhn D, Orłowski R, et al. (2011) In vitro and in vivo selective antitumor activity of a novel orally bioavailable proteasome inhibitor MLN9708 against multiple myeloma cells. *Clin Cancer Res* 17: 5311–5321.
51. Mujtaba T, Dou QP (2011) Advances in the understanding of mechanisms and therapeutic use of bortezomib. *Discov Med* 12: 471–480.
52. Groll M, Huber R, Potts BC (2006) Crystal structures of salinosporamide A (NPI-0052) and B (NPI-0047) in complex with the 20 S proteasome reveal important consequences of β -lactone ring opening and a mechanism for irreversible binding. *J Am Chem Soc* 128: 5136–5141.



Roles of conserved Arg⁷² and Tyr⁷¹ in the ascorbate-specific transmembrane electron transfer catalyzed by *Zea mays* cytochrome *b*₅₆₁

Motiur Md. Rahman,¹ Nobuyuki Nakanishi,¹ Yoichi Sakamoto,² Hiroshi Hori,^{2,3} Toshiharu Hase,⁴ Sam-Yong Park,⁵ and Motonari Tsubaki^{2,*}

Department of Molecular Science and Material Engineering, Graduate School of Science and Technology, Kobe University, 1-1 Rokkodai-cho, Nada-ku, Kobe, Hyogo 657-8501, Japan,¹ Department of Chemistry, Graduate School of Science, Kobe University, 1-1 Rokkodai-cho, Nada-ku, Kobe, Hyogo 657-8501, Japan,² Center for Quantum Science and Technology under Extreme Conditions, Osaka University, 1-3 Machikaneyama-cho, Toyonaka, Osaka 560-8531, Japan,³ Institute for Protein Research, Osaka University, Suita, Osaka 565-0871, Japan,⁴ and Division of Science of Biological Supramolecular Systems, Graduate School of Integrated Science, Yokohama City University, Yokohama, Kanagawa 230-0045, Japan⁵

Received 16 September 2012; accepted 19 November 2012
Available online 3 January 2013

Cytochromes *b*₅₆₁, novel transmembrane electron transport proteins residing in eukaryotic cells, have a number of common features including six transmembrane α -helices and two heme ligation sites. Our recent studies on recombinant *Zea mays* cytochrome *b*₅₆₁ suggested that concerted proton/electron transfer mechanism was functioning in plant cytochromes *b*₅₆₁ as well and that conserved Lys⁸³ on a cytosolic loop had important roles for ascorbate-binding and a succeeding electron transfer. In the present study, we conducted site-directed mutagenesis analyses on conserved Arg⁷² and Tyr⁷¹. Removal of a positive charge at Arg⁷² did not affect significantly on the final heme reduction level with ascorbate as reductant. However, characteristic pH-dependent initial time-lag upon electron acceptance from ascorbate was completely lost for R72A and R72E mutants. Substitution of Tyr⁷¹ with Ala or Phe affected both on the final heme reduction level and on the pH-dependent initial time-lag, causing acceleration of the electron transfer. These observations were interpreted as existence of specific interactions of Tyr⁷¹ and Arg⁷² with ascorbate. However, their mechanistic roles were distinctly different from that of Lys⁸³, as exemplified by K83A/Y71A double mutant, and might be related for expelling of monodehydroascorbate radical from the substrate-binding site to prevent a back-flow of electrons.

© 2012, The Society for Biotechnology, Japan. All rights reserved.

[Key words: Cytochrome *b*₅₆₁; Ascorbate; Monodehydroascorbate radical; Transmembrane electron transfer; Membrane protein]

During the past several decades, evidence has accumulated on the presence of specific high-potential ascorbate-reducible *b*-type cytochrome in the plasma membranes of higher plants (1–4). The cytochrome is named as cytochrome *b*₅₆₁ based on the similarities, such as α -band peak at 561 nm, reducibility with ascorbate, and positive midpoint potentials (+110–160 mV), to the *b*-type cytochrome present in chromaffin granules (CG) of animal cells (5–7). Of particular interest are recent discoveries of a number of plant genes that encode transmembrane proteins having striking homology to mammalian adrenal CG cytochrome *b*₅₆₁ (8). These cytochromes *b*₅₆₁ residing in large variety of eukaryotic cells, including Dcytb identified in the duodenal plasma membrane (9), Lcytb (10), and 101F6 (11,12), were found to constitute a novel class of transmembrane electron transport proteins (13).

A number of highly relevant structural features, including six hydrophobic transmembrane α -helices, two heme ligation sites, and possible ascorbate (AsA) and monodehydroascorbate (MDA) radical binding sequences (7,14–16), are almost perfectly conserved among the members of animal and plant cytochrome *b*₅₆₁ subfamilies. It was postulated that two heme *b* prosthetic groups are located near the putative AsA-binding sequence on the cytosolic side and the putative MDA radical-binding sequence on the intravesicular side to perform a unique transmembrane electron transfer (13,14). In the case of bovine adrenal CG cytochrome *b*₅₆₁, this postulation was verified using various biochemical and biophysical techniques (15–17). Particularly, our pulse radiolysis experiment on the purified sample in a detergent-solubilized state showed conclusively that the high-potential heme on the intravesicular side has a role for the fast electron donation to MDA radical whereas the low-potential heme on the cytosolic side is responsible for the electron acceptance from AsA (18). Further, our stopped-flow analysis on the diethylpyrocarbonate (DEPC)-modified cytochrome *b*₅₆₁ confirmed that the low-potential heme on the cytosolic side is the site for the entrance of electrons from AsA, even though both hemes can be theoretically accessible by AsA in the

* Corresponding author. Tel./fax: +81 78 803 6582.

E-mail address: mtsubaki@kobe-u.ac.jp (M. Tsubaki).

Abbreviations: AsA, ascorbate; CG, chromaffin granule; DEPC, diethylpyrocarbonate; EPR, electron paramagnetic resonance; MALDI-TOF, matrix assisted laser desorption/ionization-time of flight; MDA, monodehydroascorbate; β -OG, *n*-octyl- β -D-glucoside; Zmb₅₆₁, *Zea mays* cytochrome *b*₅₆₁.

detergent-solubilized state (17). Thus, clarification of the molecular mechanism for such site-specificity is our current interest.

For plant cytochromes b_{561} , however, there have been only a few detailed studies being conducted. This is primarily due to the difficulty in the purification from plant tissues (1,2,19). However, recent progress in the studies on plant cytochromes b_{561} suggested that they utilize AsA as a physiological electron donating substrate (20–22) to supply electron equivalents *via* transmembrane electron transfer to other reactions operative on the opposite side of the membranes. For the physiological functions of the plant cytochrome b_{561} , two possibilities might be raised. As one possible role, it might utilize AsA as the physiological substrate on the cytosolic side to regenerate AsA on the other side of membranes, as found for adrenal CG cytochrome b_{561} (23). Such regenerated AsA on the other side of membranes might be used for cell growth and cell division and/or coupling to other redox proteins (3,21). The other possibility is that plant cytochrome b_{561} might work as a transmembrane ferrireductase to reduce ferric ion to ferrous state (22) and have an indirect role for the cellular iron absorption (or storage), as proposed for Dcytb (9). Indeed, it was shown that a member of cytochrome b_{561} family had a ferrireductase activity more or less (24,25). However, since the sub-cellular and tissue-specific localization of plant cytochromes b_{561} was still not completely understood (20,21,26,27), it might be too early to make conclusive arguments. For the better understanding of exact physiological role(s) of these unique plant membrane proteins,

detailed studies concerning the molecular mechanism of transmembrane electron transfer reaction might be required.

Recently, we have succeeded in the construction of a heterologous expression system for *Zea mays* cytochrome b_{561} (Zmb_{561}) (Fig. 1) using methylotrophic yeast *Pichia pastoris* cells, established its purification procedure, and opened a new way for detailed biochemical and biophysical analyses (28,29). Our analysis using stopped-flow and pulse radiolysis techniques indicated that purified wild-type *Z. mays* cytochrome b_{561} (WT- Zmb_{561}) protein had significant activities for the electron donation to MDA radical and the electron acceptance from AsA (29). Further, our comparative study on WT- Zmb_{561} with bovine adrenal CG cytochrome b_{561} using a site-specific chemical modification technique demonstrated that the concerted proton/electron transfer mechanism, which was hypothesized to be operative in bovine adrenal CG cytochrome b_{561} upon electron acceptance from AsA (30), was clearly working in Zmb_{561} as well (31). We also performed a site-directed mutagenesis study on Zmb_{561} with particular interests on the conserved amino acid residues residing in the putative AsA and MDA radical binding sequences (29). Among the mutants examined, three site-directed mutants, K83A, K83E, and K83D, showed a significant decrease in their electron accepting ability from AsA, indicating that the well-conserved Lys⁸³ has a very important role for the binding of and the electron transfer from AsA (29).

In the present study, we focused on two amino acid residues (Tyr⁷¹ and Arg⁷²) residing in the same loop with that of Lys⁸³ as

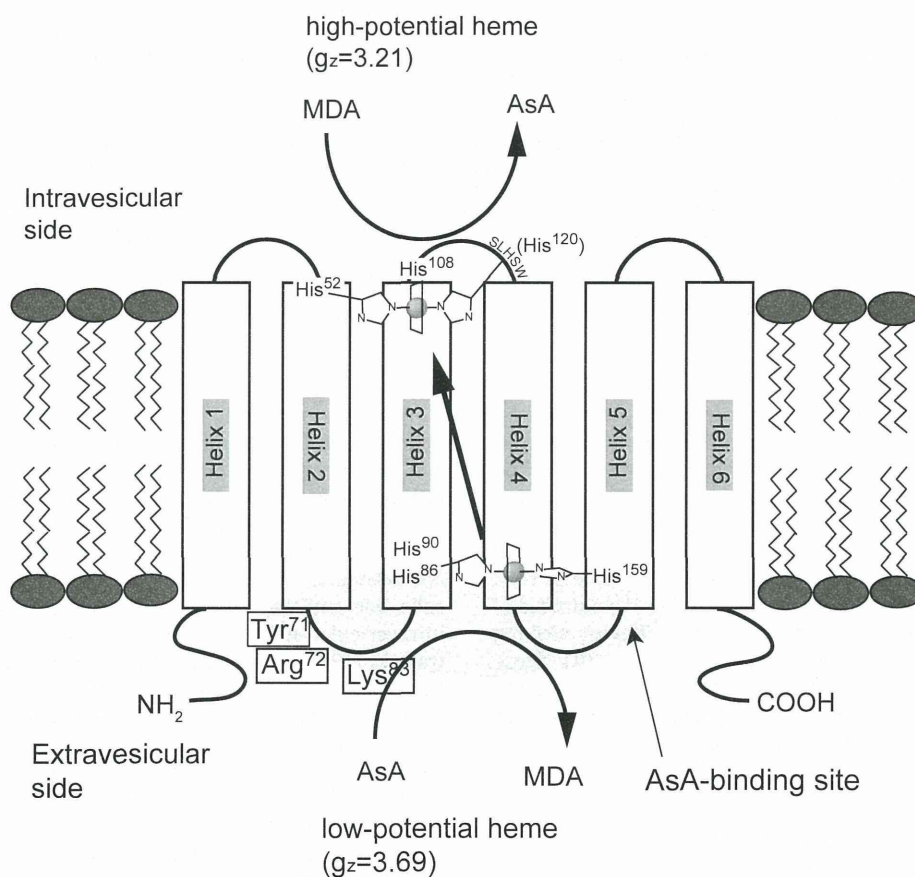


FIG. 1. The six transmembrane helices model of *Zea mays* cytochrome b_{561} . *Zea mays* cytochrome b_{561} (Zmb_{561}) is considered to have six transmembrane helices and two hemes b centers. Two hemes are located on the intravesicular and extravesicular side, respectively, with different electron paramagnetic resonance (EPR) characters as indicated based on Nakanishi et al. (31). Two well-conserved sequences (ALLVYRVFR, SLHSW) found initially in animal species were predicted as a part of the AsA- and MDA radical-binding site, respectively (14). The latter is also well conserved in plant species and is indicated in a loop connecting helix 3 and 5. On the other hand, the former sequence residing in a loop connecting helix 2 and 3 is partially conserved in plant species. However, both Tyr⁷¹ and Arg⁷² are well conserved and are expected to have important roles for the electron acceptance from AsA together with well conserved Lys⁸³ (29).

targets for the detailed site-directed mutagenesis study (Fig. 1). Both Tyr⁷¹ (corresponding to Tyr⁷³ of bovine adrenal CG cytochrome *b*₅₆₁) and Arg⁷² are located within a part of motif1 (13) and putative AsA-binding sequence (14) (Fig. 1). Since the conservation of Tyr⁷¹ is very high and is one of a few aromatic residues close to the cytosolic heme center, it may have very important roles for the electron accepting reaction from AsA. Thus, we constructed two site-directed mutants, Y71A-H₆ and Y71F-H₆. The second target, Arg⁷², probably has more important roles in the putative AsA-binding sequence (14). The positive charge of this side-chain group might be participating in a direct interaction with a negatively-charged AsA molecule, in collaboration with other positively-charged residues including Lys⁸³ (29), which might have a guiding role for the approach of AsA to the substrate-binding site on the cytosolic side (Fig. 1). Further, AsA-dependent reduction level assay on the site-directed mutants R72A of recombinant mouse adrenal CG cytochrome *b*₅₆₁ in the yeast membrane fraction (32) and of recombinant bovine adrenal CG cytochrome *b*₅₆₁ in a purified state (33) indicated the importance of a positive charge for the high-affinity AsA-binding. However, for the recombinant *Arabidopsis thaliana* cytochrome *b*₅₆₁, its K70A mutant (the corresponding position to Arg⁷² of Zmb₅₆₁) was replaced with Lys in the *Arabidopsis* cytochrome *b*₅₆₁ in yeast microsomal membranes did not show any such effects (34). To solve the apparently contradictory results, we constructed four site-directed mutants, namely, R72A-H₆, R72D-H₆, R72E-H₆ and R72K-H₆. We performed detailed biochemical and biophysical analyses on each of the site-directed mutants in a highly purified state to investigate the physiological and mechanistic roles of these two conserved residues on the cytosolic side for the transmembrane electron transfer reaction.

MATERIALS AND METHODS

Site-directed mutagenesis The cloned full-length Zmb₅₆₁ (AB182641; DDBJ/EMBL/GenBank) was ligated into *EcoR* I-*Xba* I site of pPICZB vector, as described previously (29). We further introduced a hexa-histidine (6x His) sequence at the 3' end of the Zmb₅₆₁ gene (29). The resulting expression vector, pPICZB-WT-Zmb₅₆₁-H₆, could express recombinant Zmb₅₆₁ protein with a C-terminal 6x His sequence (WT-Zmb₅₆₁-H₆). The amino acid sequence of its C-terminal part was, therefore, ²¹¹GASVVVAIAIPVRLPEPQGYDPIPEHHHHHH²⁴². Site-specific mutations were, then, introduced using Quikchange II site-directed mutagenesis kit (Stratagene Corp., La Jolla, CA, USA). All the primers, which were used for the mutagenesis, are listed in Table S1. Expression vectors for six site-specific mutants with a C-terminal 6x His-tag moiety (R72A-H₆, R72D-H₆, R72E-H₆, R72K-H₆, Y71A-H₆, and Y71F-H₆) were, thus, constructed. Construction of the expression vector for K83A/Y71A was conducted by introducing a second site-specific mutation on the expression vector for K83A mutant (29) using Quikchange II site-directed mutagenesis kit. These constructs were each confirmed by DNA sequencing using an ABI 3100 Genetic Analyzer (Applied Biosystems, Foster City, CA, USA).

Expression of Zmb₅₆₁ mutants in *P. pastoris*, cells The expression and purification of Zmb₅₆₁ mutants were followed by the procedure as described in our previous studies (28,29).

Purification of Zmb₅₆₁ mutants The expressed WT-Zmb₅₆₁-H₆ and its site-specific mutants were purified as previously described (28,29,31). Purification of K83A/Y71A was conducted as previously described (29). SDS-PAGE analysis was performed using 15% gels according to the method of Laemmli (35). The concentration of the purified Zmb₅₆₁ samples was each determined spectrophotometrically using a difference extinction coefficient of 27.7 mM⁻¹ cm⁻¹ at 561 nm minus 575 nm in the reduced state (7).

Matrix assisted laser desorption/ionization-time of flight (MALDI-TOF)-mass spectrometry Mass spectrometric analyses were conducted with a Voyager DE Pro mass spectrometer (Applied Biosystems, Foster City, CA, USA) using a 20-kV accelerating voltage. Other experimental conditions were essentially the same as in previously described (15,16,29). All of the recombinant wild-type protein (WT-Zmb₅₆₁-H₆) and its site-specific mutants (Y71A-H₆, Y71F-H₆, R72A-H₆, R72D-H₆, R72E-H₆, R72K-H₆, and K83A/Y71A) (~100 μM) were each digested either with TPCK-treated trypsin (0.01 mg/mL) or *Staphylococcus aureus* V8 protease (0.01 mg/mL), respectively. After 48 h of incubation at room temperature, the peptide solutions were diluted 1:9 (v/v) with a matrix solution (α -cyano-4-hydroxycinnamic acid (Aldrich, Gillingham, England), 50 mg/mL in 50% acetonitrile in 0.3% TFA). The mixtures (typically, 1.0 μL) were deposited on

a sample plate, allowed to air-dry, and analyzed. The search of the corresponding fragments in the amino acid sequence of Zmb₅₆₁ mutants was conducted using the program GPMW (v 6.11) (Lighthouse Data, Odense M, Denmark).

Electron paramagnetic resonance (EPR) spectroscopy Purified Y71A and WT-Zmb₅₆₁ samples (200–300 μM) in 50 mM potassium phosphate (pH 7.0) buffer containing 1.0% (w/v) *n*-octyl- β -D-glucoside (β -OG) were introduced into EPR tubes and were frozen in liquid nitrogen (77 K) immediately. EPR measurements were carried out at X-band (9.23 GHz) microwave frequency using a Varian E-12 EPR spectrometer with 100-kHz field modulation, as previously described (7,29).

AsA-reduction level assay Eight purified Zmb₅₆₁ mutants (Y71A-H₆, Y71F-H₆, R72A-H₆, R72D-H₆, R72E-H₆, R72K-H₆, K83A, and K83A/Y71A) and wild-type protein (WT-Zmb₅₆₁-H₆) were each diluted to 1 μM with 50 mM potassium-phosphate buffer (pH 7.0, 6.0) or 50 mM sodium acetate buffer (pH 5.0) each containing 1.0% (w/v) β -OG. After 30 min of incubation at room temperature, UV-visible absorption spectra of the mutants in oxidized and dithionite-reduced states were measured from 700 to 200 nm with a UV-2400PC spectrophotometer (Shimadzu Corp., Kyoto, Japan). For the AsA-reduced state of the mutants, the absorbance change at 425 nm was recorded for 30 min after the addition of AsA (10 mM) although the equilibrium was attained within 30 s after the addition. Then, the spectra were measured. The final reduction level with AsA as a reductant was calculated based on the dithionite-reduced form as the 100% reduction level.

Redox titrations Spectroscopic titrations were performed as described by Dutton (36) and Takeuchi (16), using a Shimadzu UV-2400PC spectrometer equipped with a thermostated cell holder connected to a low temperature thermobath (NCB-1200, Tokyo Rikakikai Co, Ltd, Tokyo, Japan). During the measurements, visible absorption spectra and redox potentials were recorded in an appropriate interval, as previously described (29). The changes in absorbance (*A*_{561.0} minus *A*_{566.8}, the latter corresponding to the isosbestic point of WT-Zmb₅₆₁-H₆) were corrected with the dilution effect and analyzed with Igor Pro (v. 6.03A2) employing a Nernst equation with two redox components; i.e., with a linear combination of two sigmoid functions;

$$f(x) = \text{base} + (\text{max} * 1 / (1 + \exp((x1 - x) / \text{slope} 1))) + (\text{max} * 2 / (1 + \exp((x2 - x) / \text{slope} 2))) \quad (1)$$

in which base, max, slope 1, and slope 2 were fixed as 100, -50, 25.62, and 25.62, respectively, during the curve-fitting procedure, and $\times 1$ and $\times 2$ gave the estimated midpoint potentials (in mV), respectively. Potentials are expressed relative to the normal hydrogen electrode (NHE).

Stopped-flow analyses Rapid kinetic measurements were carried out using an RSP-1000-03DR stopped-flow spectrometer (Unisoku, Osaka, Japan). Purified WT-Zmb₅₆₁-H₆ or either of its site-directed mutants (Y71A-H₆, Y71F-H₆, R72A-H₆, R72D-H₆, R72E-H₆, R72K-H₆, K83A, and K83A/Y71A) in oxidized state was each diluted to 2 μM with 50 mM potassium-phosphate buffer (pH 7.0, 6.0) or 50 mM sodium acetate buffer (pH 5.0) each containing 1.0% (w/v) β -OG. After 30 min of incubation at room temperature, protein solution and AsA solution were loaded into a different chamber of the apparatus, respectively. The temperature of both chambers was maintained at 20°C by connecting to a thermobath. Mixing of the two solutions was carried out with a 1:1 volume ratio and the heme absorbance change at 427 nm due to the reduction with AsA was recorded against time. Data points were collected in every 250 μs for the measurements of time duration of 1 s and in every 2.5 ms and 15 ms for the measurements of time duration of 10 s and 60 s, respectively. Both Igor Pro software (v. 6.03) and a built-in software of the stopped-flow apparatus were used for data analyses. For the measurements of K83A and K83A/Y71A, the samples without 6x His-tag moiety were used. We found previously that presence of 6x His-tag moiety of WT-Zmb₅₆₁ did not cause any significant influences on the electron transfer from AsA (29,31). Other experimental conditions were described previously (29,31).

RESULTS

MALDI-TOF-mass spectrometric analyses and visible absorption spectra of purified *Z. mays* cytochrome *b*₅₆₁ and its site-specific mutants Purified recombinant wild-type proteins (WT-Zmb₅₆₁-H₆ and WT-Zmb₅₆₁) and their site-directed mutants (Y71A-H₆, Y71F-H₆, R72A-H₆, R72D-H₆, R72E-H₆, R72K-H₆, K83A, and K83A/Y71A) were each examined by MALDI-TOF-mass spectrometry to verify the site-specific mutations (Tables S2–S7, Figs. S1–S7). All the purified samples showed characteristic visible absorption spectra as a member of the cytochrome *b*₅₆₁ family, with peaks at 414 nm for the oxidized form and at 561, 529, and 427 nm for the dithionite-reduced form. As a representative example, UV-visible spectra of R72A-H₆ mutant in oxidized, AsA-reduced, and dithionite-reduced states are shown in Fig. 2A, indicating close similarities to those of WT-Zmb₅₆₁ (29) and of bovine adrenal CG cytochrome *b*₅₆₁ (7) (for other mutants, spectra not

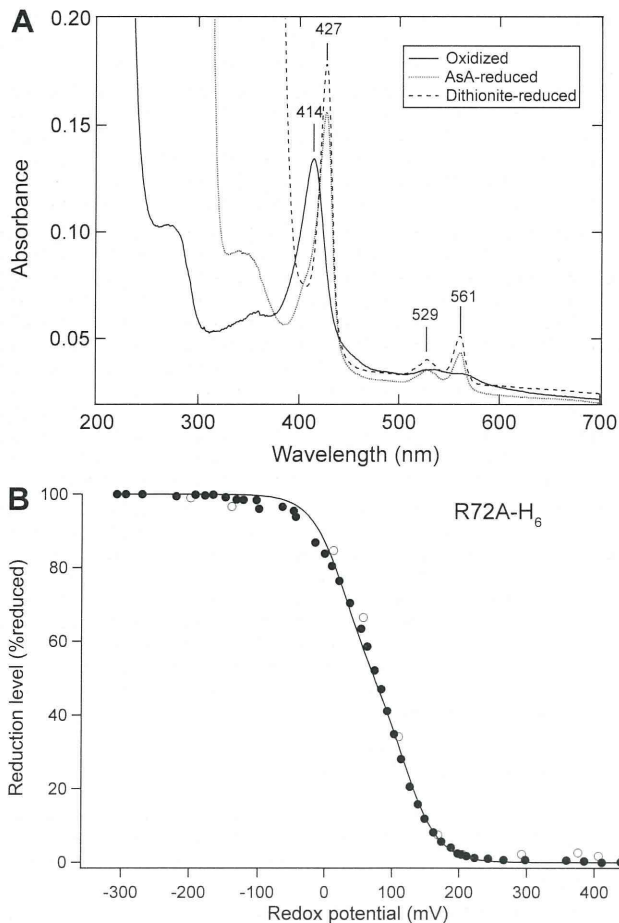


FIG. 2. Absorption spectra of oxidized, AsA-reduced and dithionite-reduced forms of R72A-H₆ (A) and potentiometric behaviors of R72A-H₆ by the least-square curve-fitting analysis (B). (A) After 30 min of incubation of R72A-H₆ with AsA (10 mM) in 20 mM Na-phosphate buffer (pH 7.0), 1.0% (w/v) β -OG, its UV-visible absorption spectrum was recorded and was compared with those in oxidized and in dithionite-reduced states. (B) Percentages of the reduction level of R72A-H₆ vs. redox potential were calculated based on the absorbance difference of α -band peak (561.0 nm) and an isosbestic point (567.2 nm). Solid and open circles indicate data points for the reductive and the oxidative titrations, respectively. A least-square curve-fitting on the data points of the reductive phase was conducted by assuming two distinct redox components; i.e., with a linear combination of two sigmoid functions. Other details are described in the text.

shown). These results suggested that all the mutations introduced did not affect significantly on the overall structure of the Zmb₅₆₁ molecule or even the local structure around the immediate surroundings of two heme *b* prosthetic groups.

EPR spectroscopy EPR spectrum measured at 5 K of oxidized Y71A, which was chosen as a representative example for evaluation of the mutation in the cytosolic loop, showed a g_z -signal from a low-spin heme with the HALS (highly anisotropic low-spin) character (37) and a g_z -signal from the other heme with the rhombic character. The former EPR signal, assigned to the cytosolic heme center (7), was actually composed of two signals with slightly different g_z values ($g_z = 3.70$ and 3.59) (Fig. S8), in which the latter signal ($g_z = 3.59$) was not observed in those of oxidized WT-Zmb₅₆₁ and K83A measured at 5 K (29). On the other hand, the other low-spin heme signal ($g_z = 3.15$) assignable to the intravesicular heme center (7) lost its relative intensity slightly compared to those of WT-Zmb₅₆₁ and K83A mutant (29). When measured at 15 K, a new low-spin EPR species with $g_z = 2.90$ and $g_y = 2.27$ signals dominated in the spectrum (Fig. S8).

The pH-dependent behavior of the final reduction level To evaluate overall influences of the mutations introduced, we investigated the final heme reduction level with AsA (10 mM) as a reductant at three different pH (Fig. 3A and B). At pH 7.0, addition of AsA (10 mM) to the oxidized WT-Zmb₅₆₁-H₆ caused a quick reduction of heme *b* reaching the final reduction level of $\sim 80\%$, as previously reported (29,31), being consistent with the notion that Zmb₅₆₁ utilize AsA as a physiological reductant in *Z. mays* cells. Four site-specific mutants (R72A-H₆, R72D-H₆, R72E-H₆, and R72K-H₆) for Arg⁷², which is located on the cytosolic side of the molecule, did not show any significant changes in the final heme reduction level nor any significant pH-dependency (Fig. 3A). On

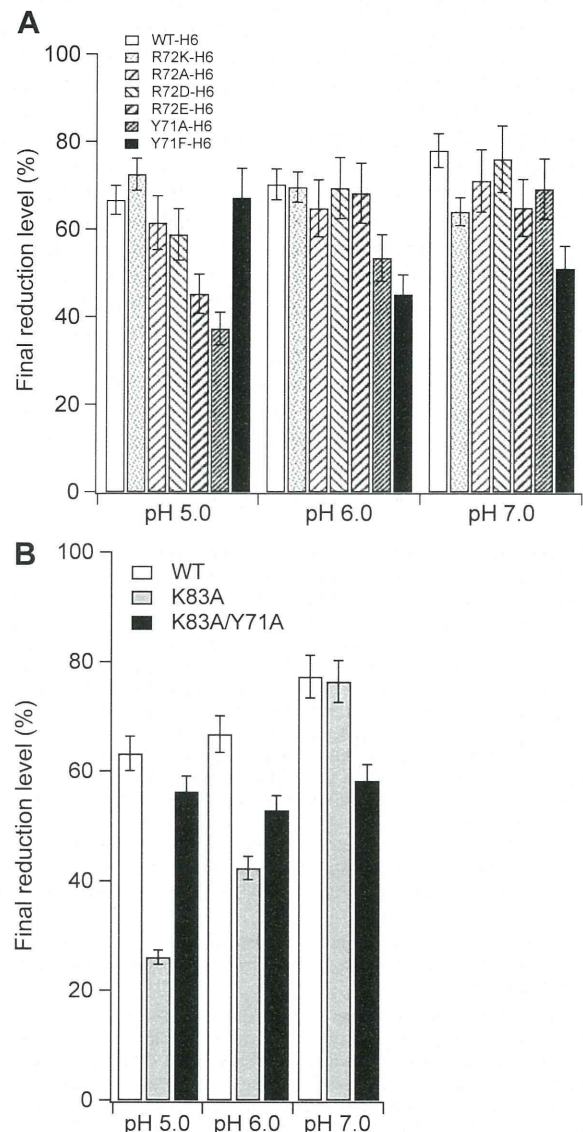


FIG. 3. Effects of pH change on the final heme reduction levels of WT-Zmb₅₆₁-H₆ and WT-Zmb₅₆₁ and their mutants using AsA as a reductant. (A) After 30 min of incubation of WT-Zmb₅₆₁-H₆, R72A-H₆, R72D-H₆, R72E-H₆, Y71A-H₆, and Y71F-H₆ with AsA (10 mM) in buffer containing 1.0% (w/v) β -OG with three different pH (5.0, 6.0, and 7.0) at room temperature, their respective UV-visible absorption spectrum was recorded and was compared with those in oxidized and in the dithionite-reduced states. The final heme reduction levels with AsA as a reductant were calculated from the spectra based on the dithionite-reduced form as the 100% level. (B) After 30 min of incubation of WT-Zmb₅₆₁, K83A, and K83A/Y71A with AsA (10 mM) in buffer containing 1.0% (w/v) β -OG with three different pH (pHs 5.0, 6.0, and 7.0) at room temperature, their respective UV-visible absorption spectrum was recorded and was compared with those in oxidized and in the dithionite-reduced states.

the other hand, Y71A-H₆ mutant showed a much lower heme reduction level than those of WT-Zmb₅₆₁-H₆ with AsA at pH 5.0, indicating slight pH-dependent changes (Fig. 3A). Y71F-H₆ mutant showed a very different property from those of WT-Zmb₅₆₁-H₆ and other mutants. It showed a very high reduction level at pH 5.0, whereas, at pH 6.0 and 7.0, the reduction level became lowered than the others (45–50%) (Fig. 3A).

Very interestingly, upon analysis of K83A/Y71A double mutant, we found that the significant lowering of heme reduction level caused by the K83A mutation at pH 5.0 (29) was apparently rescued by introducing a second mutation of Y71A (Fig. 3B).

Effects of mutations on the redox potentials of Zmb₅₆₁ As previously reported (29), the apparent midpoint potential of WT-Zmb₅₆₁-H₆ was estimated as +66 mV and midpoint potentials of the higher and the lower redox components showed +119 and +11 mV, respectively, after the curve-fitting analysis with a least-square method assuming two distinct redox components (Table 1). We confirmed further that there was no distinct effect upon removal of the 6x His-tag moiety (for WT-Zmb₅₆₁; apparent midpoint potential, +64 mV; higher and lower redox components as +118 and +9 mV, respectively) (Table 1). Mutations of Arg⁷² did not affect significantly on the redox potentials of both heme centers (Table 1). A typical example (for R72A-H₆) is shown (Fig. 2B). On the other hand, mutations of Tyr⁷¹ did affect significantly on both heme centers; the center with a higher redox potential showed a decrease by 30–40 mV, whereas the center with a lower redox potential showed a significant decrease by ~10 mV for Y71A-H₆ and ~80 mV for Y71F-H₆ (Table 1). Results of the analyses for Y71A-H₆ and Y71F-H₆ are shown in (Figs. S9 and S10), respectively. The K83A/Y71A mutant showed similar redox potentials with those of Y71A-H₆ (Table 1) rather than those of K83A (29).

Stopped-flow analyses of WT-Zmb₅₆₁-H₆ and its site-specific mutants

The electron accepting reaction of oxidized WT-

Zmb₅₆₁-H₆ and its site-directed mutants were analyzed by stopped-flow spectrometry (Fig. 4A). As a representative example, the absorbance change at 427 nm after mixing of oxidized WT-Zmb₅₆₁-H₆ (final, 1 μM) with AsA (final, 2 mM) was presented against time in a logarithmic scale (Fig. 4Aa). The result showed that, in the initial phase of the electron acceptance from AsA, the heme reduction rate of WT-Zmb₅₆₁-H₆ was much slower at pH 5.0 than that measured at pH 7.0, as observed for bovine adrenal CG cytochrome *b*₅₆₁ (17) and for WT-Zmb₅₆₁ (29). On the other hand, such an initial time-lag at pH 5.0 was almost completely absent for R72A-H₆ (Fig. 4Ab) and R72E-H₆ (Fig. 4Ad) mutants. For R72D-H₆ mutant, the initial time-lag at pH 5.0 still persisted but with a much reduced extent (Fig. 4Ac). It might be stressed that there were not so much pH-dependency in the initial apparent rate constants for the R72A-H₆ and R72E-H₆ mutants and these values were very similar to those of WT-Zmb₅₆₁-H₆ measured at pH 6.0 (Fig. 4Aa).

Time-courses of the reduction process with AsA for both Y71A-H₆ and Y71F-H₆ mutants were also analyzed by stopped-flow spectrometry. In the case of Y71A-H₆, the initial time-lag at pH 5.0 was almost absent (Fig. 4Ae). Further, overall reduction process of Y71A-H₆ with AsA was similar to (or even faster than) those of R72A-H₆ (Fig. 4Ab) and R72E-H₆ (Fig. 4Ac) mutants. Surprisingly, acceleration of the electron transfer from AsA to the heme at pH 5.0 was clearly seen for Y71F-H₆ mutant (Fig. 4Af) when compared with the time-courses of WT-Zmb₅₆₁-H₆ and the R72 mutants.

For clarification of these analyses, we also calculated the apparent rate constants (k_{app} (sec⁻¹)) of the reduction processes corresponding to the plotted data in Fig. 4A and the results are tabulated in Table S8. For the calculation, we assumed a single exponential decay for the initial 10 s and 60 s after the mixing with AsA for the simplicity. This treatment was based on the notion that the entire reduction of Zmb₅₆₁ is actually composed of two succeeding steps; i.e., an initial fast electron accepting reaction from AsA at the cytosolic heme and a following slow long-range electron transfer from the reduced cytosolic heme to the oxidized intravesicular heme (17,18). It is obvious from Table S8 that, at pH 5.0, WT-Zmb₅₆₁-H₆ and R72D-H₆ showed much smaller k_{app} values compared to those of R72A-H₆, R72E-H₆, and Y71A-H₆. On the other hand, Y71F-H₆ showed distinctly large k_{app} values at pH 5.0, about 7–8 times larger than the corresponding values of WT-Zmb₅₆₁-H₆ and 3–4 times larger than those of R72D-H₆, R72E-H₆, Y71A-H₆. Thus, from the data in Fig. 4A and Table S8, we can conclude that the substitutions of Arg⁷² (with Ala or Asp) and Tyr⁷¹ (with Ala or Phe) caused a significant suppression of the characteristic pH-dependent time-lag upon the electron acceptance from AsA, leading to the faster electron acceptance from AsA at acidic pH. In the case of the substitution of Tyr⁷¹ with Phe, there was actually a significant acceleration of the electron transfer from AsA (Table S8). These observations indicated some important roles of Tyr⁷¹ for the electron transfer from bound AsA.

Stopped-flow analyses of the Y71A/K83A double mutant

The Y71A/K83A double mutant showed fast electron accepting reactions from AsA irrespective of pH (Fig. 4Bb, Table S9). It was noteworthy that there was no apparent initial delay even at pH 5.0 (Fig. 4Bb). This behavior was very similar to those of Y71A-H₆ and R72A-H₆ mutants (Fig. 4A). These results confirmed that the significant lowering of the electron accepting ability caused by the K83A mutation (29) was rescued by introducing the second mutation of Y71A. However, the original pH-dependency as found for wild-type Zmb₅₆₁-H₆ (Fig. 4Aa) [or in WT-Zmb₅₆₁ (29) and adrenal CG cytochrome *b*₅₆₁ (17)] was lost almost completely for its compensation.

TABLE 1. Redox potentials of Zmb₅₆₁ and effects of site-specific mutations on the redox properties in comparison with those of bovine adrenal CG cytochrome *b*₅₆₁.

Cytochromes	Apparent midpoint potential (mV)	Slope ^a	Estimated higher midpoint potential ^b (mV)	Estimated lower midpoint potential ^b (mV)
WT-Zmb ₅₆₁	+65.6	46.4	+118.9	+11.3
WT-Zmb ₅₆₁ -H ₆	+64.0	46.3	+118.2	+8.5
R72A-H ₆	+76.5	41.3	+119.9	+27.3
R72D-H ₆ ^c	ND	ND	ND	ND
R72E-H ₆	+52.7	49.1	+110.5	-6.2
R72K-H ₆	+62.7	51.9	+126.2	-1.3
Y71A-H ₆	+41.8	39.2	+83.8	0.0
Y71F-H ₆	+10.6	61.7	+76.7	-74.7
K83A/Y71A	+37.7	36.4	+78.3	-0.6
K83A ^d	+44.8	41.5	+93.0	-4.4
Bovine CG	+125	—	+170	+60
<i>b</i> ₅₆₁ ^e				
Bovine CG	+128	—	+170	+70
<i>b</i> ₅₆₁ ^f				

^a Slope values were defined as variables during the fitting procedure using a single sigmoidal function and are, therefore, corresponding to the slope of the curvature.

^b For the curve-fitting procedure using two independent sigmoidal functions, slope value for each sigmoidal function was fixed as 25.619 and is, therefore, not indicated.

^c Due to the instability of the purified protein at room temperature, reliable redox potential measurements could not be performed and, therefore, these values were not determined (ND).

^d From Nakanishi et al. (29) for Zmb₅₆₁ without the His-tag moiety.

^e From Apps et al. (53) for the purified form obtained from bovine adrenal gland.

^f From Takeuchi et al. (16) for the purified form obtained from bovine adrenal gland CG.

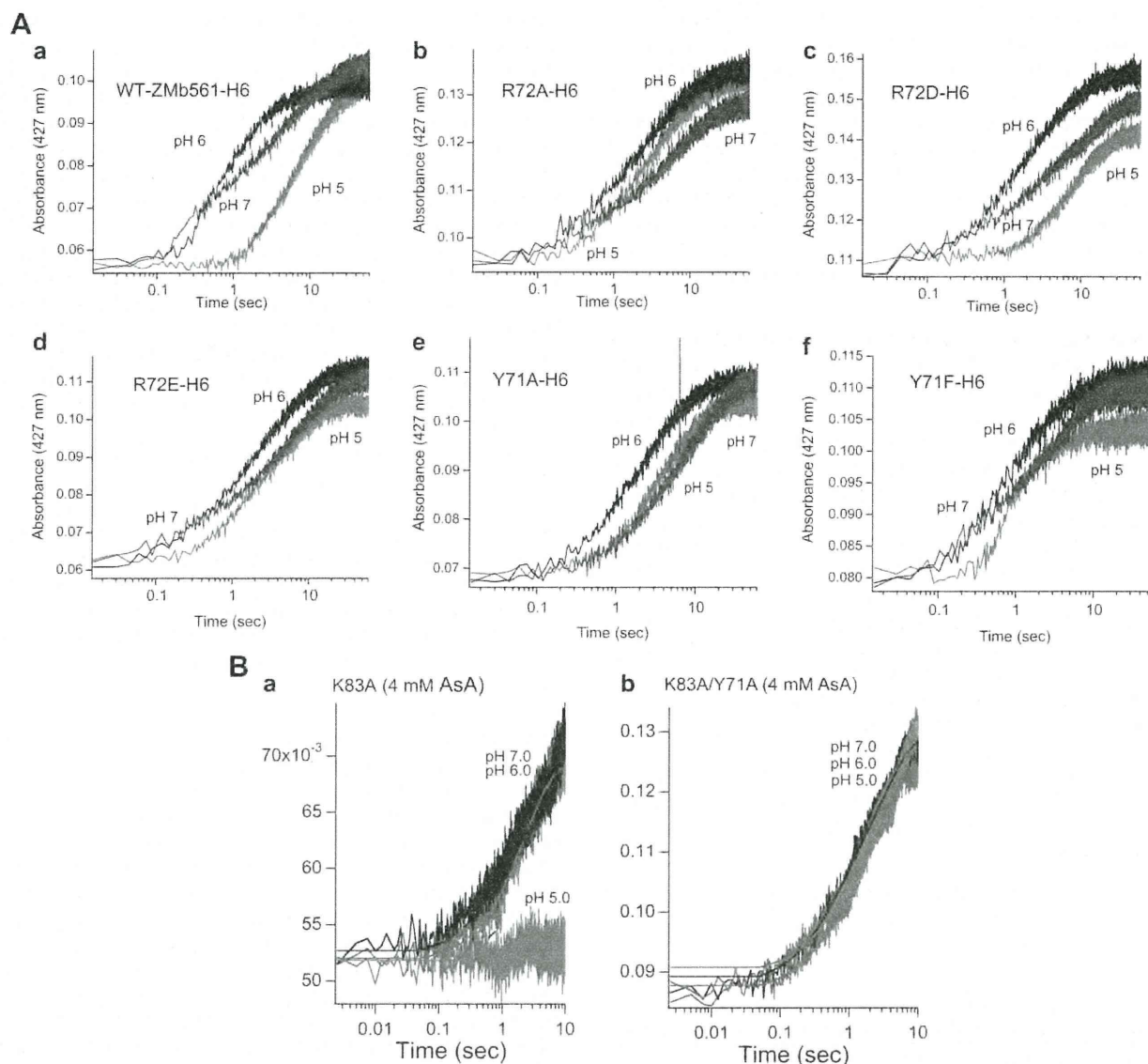


FIG. 4. (A) Stopped-flow analyses of the electron transfer from AsA for the purified WT-Zmb₅₆₁-H₆, its R72 mutants (R72A-H₆, R72D-H₆, R72E-H₆), and Y71 mutants (Y71A-H₆, Y71F-H₆) measured at three different pH. (B) Stopped-flow analyses of the electron transfer from AsA for the purified WT-Zmb₅₆₁, K83A, and K83A/Y71A mutants measured at three different pH. (A) The electron accepting reactions of oxidized WT-Zmb₅₆₁-H₆ (a) [and its site-directed mutants; R72A-H₆ (b), R72D-H₆ (c), R72E-H₆ (d), Y71A-H₆ (e) and Y71F-H₆ (f)] (final, 1 μ M) from AsA (final, 2 mM) were measured at 427 nm and at three different pH (pHs 5.0, 6.0, and 7.0) by stopped-flow spectrometry using two solution mixing system with a 1:1 volume ratio. The absorbance changes were plotted against time in a logarithmic scale. (B) The electron accepting reactions of oxidized K83A (a) and K83A/Y71A (b) mutants (final, 1 μ M) from AsA (final, 4 mM) were measured at three different pH (pHs 5.0, 6.0, and 7.0). Other conditions including buffer conditions are the same as in panel A.

DISCUSSION

Electrochemistry of AsA and its relation to the electron transfer mechanism to the heme center of cytochrome *b*₅₆₁

Since AsA has two acidic protons ($pK_{a1} = 4.04$ and $pK_{a2} = 11.34$) (38), three species, i.e., ascorbic acid (H_2AsA), ascorbate monoanion ($HAsA^-$), and ascorbate dianion (AsA^{2-}), are present in neutral solution with the monoanion form as a predominant species. For ascorbate free radicals, monoanion form (MDA $^{\cdot-}$) is a predominant species under physiological conditions (23,38,39). Since the monoanion form ($HAsA^-$) is not a good electron donor and the scarce dianion form (AsA^{2-}) is a much powerful electron donor, it was postulated that adrenal CG cytochrome *b*₅₆₁ has such a molecular mechanism to withdraw a proton from the monoanion form to facilitate electron transfer to its oxidized heme (concerted H^+/e^- transfer

mechanism) (23). We extended the model to include an imidazole group of the cytosolic heme axial His ligand as a site for the proton acceptance (30). Our previous studies on Zmb₅₆₁ (31,40) showed that the concerted H^+/e^- transfer mechanism is operative in plant cytochrome *b*₅₆₁ as well.

For a better understanding of the efficient electron transfer reaction of Zmb₅₆₁ from AsA based on the concerted H^+/e^- transfer mechanism, we may categorize conserved amino acid residues near the AsA-binding site by considering their putative mechanistic roles; namely, (i) residues responsible for helping the approach of AsA to the AsA-binding site and for its recognition, (ii) residues responsible for the stabilization of AsA at the AsA-binding site, which may promote the electron transfer by providing a route to the oxidized heme, (iii) residues responsible for withdrawing and transferring a proton from C2-OH group of AsA, which may also provide a route for the electron transfer, and (iv) residues

responsible for expelling MDA radical from the AsA-binding site to prevent a reverse electron flow from the reduced heme center.

Our previous site-specific chemical modification studies on adrenal CG cytochrome *b*₅₆₁ suggested the importance of conserved Lys⁸⁵ (corresponding to Lys⁸³ of WT-Zmb₅₆₁-H₆) for the quick electron acceptance from AsA (15,16). More recent studies on WT-Zmb₅₆₁ and WT-Zmb₅₆₁-H₆ (31,40) indicated that Lys⁸³ had a similar high reactivity toward DEPC and such a specific DEPC-modification caused a significant retardation of the electron transfer from AsA. Mechanistic role(s) of this positively-charged residue was further analyzed by site-specific mutants, K83A, K83D, and K83E (29). Stopped-flow analyses showed that the initial time-lag phase for these mutants was much longer than that of WT-Zmb₅₆₁, causing a significant retardation of the electron transfer (29). One may propose that the initial lag-phase of the wild-type protein is due to the presence of a resting inactive state, which must first be reactivated. Although we cannot discard such a possibility completely, this view is not consistent with the results for the three Lys⁸³ mutants (29), which indicated further extension of the initial lag-phase. Therefore, the initial lag-phase might be directly related to the binding process of AsA, being consistent with the notion that a positive charge of Lys⁸³ would have an electrostatic interaction with a negatively-charged AsA molecule (17). Thus, Lys⁸³ should be classified as group A.

DEPC-treatments of WT-Zmb₅₆₁-H₆ and four site-specific mutants (Y71A-H₆, R72A-H₆, R72D-H₆, and R72E-H₆) (40) caused similar inhibitory effects on their electron acceptance from AsA as found for WT-Zmb₅₆₁ (31). DEPC-treatment of K83A mutant also showed a similar inhibition (40), in which only heme axial His residue(s) were potential major modification sites. These results suggested that the specific *N*-carbethoxylation of the heme axial His residue(s) was a major cause of the inhibition of electron acceptance from AsA. Thus, based on the concerted H⁺/e⁻ transfer mechanism at the cytosolic heme center (30), we conclude that His⁸⁶ could be classified as group C.

Possible mechanistic roles of Arg⁷² Previously, Arg⁷² was proposed as an important residue for the interaction with AsA because of its positive charge and its high conservation (32). In the past, several X-ray crystal structures for AsA-bound enzymes, including ascorbate peroxidases (41), hyaluronate lyase (42), and myrosinase (43), were reported. In all of these structures, a conserved Arg residue has essential roles for the binding of AsA at their active sites (44), in which side-chains of the Arg residues were interacted with the 2-O and 3-O atoms (41), 1-O and 2-O atoms (42), 1-O and 2-O atoms (43) of the bound AsA *via* hydrogen bonding, respectively. Further, in the engineered AsA-binding site of cytochrome *c* peroxidase by mimicking ascorbate peroxidase, an introduced Arg residue was found to form a hydrogen bond (45). Indeed, a site-directed mutagenesis study on mouse recombinant CG cytochrome *b*₅₆₁ in the yeast membrane fraction indicated that mutation of Arg⁷² to Ala abolished the high affinity heme reduction by AsA (32). Further, site-directed mutagenesis studies on Lcytb showed that mutation of Arg⁶⁷ (corresponding to Arg⁷²) to Ala resulted in an almost complete loss of the activity in the yeast cell-surface ferric reductase assay (25). These pieces of evidence seemed to suggest that Arg⁷² could be categorized as group A or group B. However, our present results on the Arg⁷² mutants did not support these observations and were not consistent with the notion that Arg⁷² provides an electrostatic interaction(s) with AsA to facilitate the electron transfer from it. Removal of the positive charge by substitution with Ala (R72A) or conversion to a negatively-charged residue by substitution with Asp (R72E) did not cause any retardation (or lowering) of the electron transfer from AsA at all at a neutral pH, when analyzed with stopped-flow

spectrometry. More interestingly, the initial time-lag observed for adrenal CG cytochrome *b*₅₆₁ (17) and WT-Zmb₅₆₁ (29) (and in the present study for WT-Zmb₅₆₁-H₆) observed at an acidic pH was completely lost in these mutants, just in an opposite direction of that seen for the Lys⁸³ mutants, although for the R72D mutant the initial time-lag was somewhat conserved and the apparent rate constants for the electron acceptance from AsA were still slower at pH 5.0 (Table S8). These results suggest that Arg⁷² has a clearly different mechanistic role(s) from that of Lys⁸³ in the electron accepting reaction from AsA. At an acidic pH, major HASA⁻ and minor H₂AsA forms are in equilibrium and, somehow, Arg⁷² stabilizes the bound AsA molecule to shift the equilibrium in favoring the H₂AsA form, as depicted in Fig. 5. In this stabilized structure, a proton (of the 2-OH group) could not be removed from AsA by His⁸⁶ *via* concerted H⁺/e⁻ transfer mechanism (Fig. 5) and, therefore, a significant initial time-lag might be observed. However, substitution of the positive side-chain with a neutral or a negative group (i.e., R72A and R72E mutants) might cause an easier release of a proton from the bound AsA leading to a faster electron transfer from AsA to the heme iron. In the case of R72D mutant, however, there was no such promoting effect, possibly due to a shorter side-chain of Asp⁷² than that of Glu⁷² of R72E.

If so, what is a mechanistic role(s) of the stabilization of the bound AsA by Arg⁷²? The most-likely explanation is that Arg⁷² may have a role to destabilize the binding of MDA monoanion (MDA⁻) radical at the AsA-binding site to prevent a reverse electron flow from the reduced heme center (Fig. 5). Although both MDA monoanion (MDA⁻) radical and ascorbate monoanion (HASA⁻) has a negative charge, fine discrimination might be possible since the former has one unpaired electron spread over a highly conjugated tricarbonyl system (39) and is presumably much planar than the latter (Fig. 5). It is quite reasonable to consider that adrenal CG cytochrome *b*₅₆₁ might also have this kind of molecular mechanism for expelling MDA radical from AsA-binding site. Since there are sufficient amounts of intravesicular (~10 mM) and cytosolic

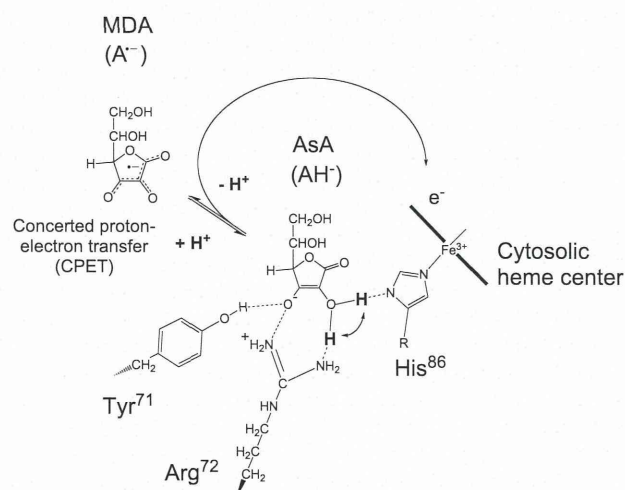


FIG. 5. Possible roles of Arg⁷², Tyr⁷¹ and His⁸⁶ in the electron transfer reaction from AsA to the cytosolic heme center of Zmb₅₆₁. We postulated that both Arg⁷² and Tyr⁷¹ have strong hydrogen bonding (or electrostatic) interactions with the bound AsA at the putative AsA-binding site. This will cause slowdown of the proton release from the bound AsA, resulting in retardation of the electron transfer from AsA to the cytosolic heme center, particularly at acidic pH. Then, release of a proton from the bound AsA would be promoted by His⁸⁶ *via* concerted H⁺/e⁻ transfer mechanism. There might be a movement (or conformational readjustment) of the bound AsA before proceeding to the next step. The physiological role of Arg⁷² and Tyr⁷¹ might be an expelling of MDA radical from the AsA-binding site to prevent a reverse electron transfer. Lys⁸³ was omitted from the scheme for the simplicity.

(~5 mM) AsA in adrenal chromaffin cells and, therefore, cytochrome b_{561} is almost in the fully-reduced state. Accordingly, prevention of the reverse electron transfer to MDA radical on the cytosolic side might be a primary importance. Such a molecular mechanism may be distributed among plant cytochromes b_{561} as well. In this case, Arg⁷² might be classified as group D rather than group B.

Possible mechanistic roles of Tyr⁷¹ For the two Tyr⁷¹ mutants, we did observe some significant influences of the mutations on the final heme reduction level with AsA, but in a different way. Y71A-H₆ showed a lower heme reduction level than those of WT-Zmb₅₆₁-H₆. On the other hand, Y71F-H₆ mutant showed a very high reduction level at pH 5.0, whereas at pH 6.0 and 7.0 its reduction level was much lower (45–50%) than that of WT-Zmb₅₆₁-H₆. Stopped-flow analysis of Y71A-H₆ mutant did not show any retardation upon the electron acceptance from AsA at a neutral pH. Importantly, again, the characteristic initial time-lag was almost absent at acidic pH. In the case of Y71F-H₆ mutant, all the steps of the electron transfer from AsA seemed to be accelerated, particularly at acidic pH. These results indicated that the mechanistic role of Tyr⁷¹ might be also very complex.

The EPR spectra of oxidized Y71A mutant measured at 5 and 15 K (Fig. S8) showed that the low-spin species with HALS character, which has been assigned to the cytosolic heme center, was actually composed of two species with slightly different g_z values ($g_z = 3.70$ and 3.59). The latter g_z -signal ($g_z = 3.59$) was not observed in those of oxidized WT-Zmb₅₆₁ and K83A mutant measured at 5 and 15 K (29). On the other hand, the other low-spin species ($g_z = 3.15$) assignable to the intravesicular heme center seemed to remain intact. These results suggested that the coordination structure of the cytosolic heme center was slightly perturbed upon the mutation of Tyr⁷¹ and such an alteration might become apparent only at low temperatures. Thus, it is tempting to propose that Tyr⁷¹ contributes to a structural role for the stabilization around the cytosolic heme center by considering its rather high conservation in many cytochromes b_{561} (13,14). The appearance of the $g_z = 2.90$ species (7,46) may indicate that such a decrease in the stability around the cytosolic heme center could be propagated further to the overall stability of Zmb₅₆₁ molecule.

Recently, however, this classical view was challenged as that the $g_z = 3.7$ signal was assignable to the low-potential intravesicular heme and *vice versa* (47–49). In this new topological model, however, there was a difficulty that the transmembrane electron transport occurs against ~100 mV gradient of the redox potentials of the two heme centers (47). Indeed, in a more recent study employing *Arabidopsis* cytochrome b_{561} being expressed in both *P. pastoris* and *Escherichia coli* cells and DEPC reagent, Cenacchi *et al.* concluded that the AsA-binding site is located near the low-potential heme (i.e., the $g_z = 3.7$ heme) and the other ferric-chelates reduction site is close to the high-potential heme (i.e., the $g_z = 3.15$ heme) (50). Accordingly, in the following discussion, we take the classical view of the heme assignments; however, even if our assignments were wrong, it would not affect the final conclusion.

Detailed analysis on the stopped-flow experiments suggested that Tyr⁷¹ has an additional role other than the structural one. Its possible role may be the destabilization of a bound MDA radical and expelling it from the AsA-binding site, similar to that of Arg⁷². In our proposed scenario, the phenol-OH group of Tyr⁷¹ in collaboration with Arg⁷² might have specific interactions with the bound AsA in favoring the H₂AsA form (Fig. 5) and, accordingly, release of the 2-OH proton from the bound AsA might be inhibited at a lower pH. Indeed, such an example for this kind interaction between a Tyr residue and a bound AsA is proposed for a plant heme oxygenase (44). For a planar MDA radical without the 2-OH group [i.e., mon-anion form (MDA⁻)], Tyr⁷¹ would not have any preference and the

MDA radical might be expelled from the AsA-binding site and, therefore, the reverse electron transfer would be inhibited. Substitution of Tyr⁷¹ with Ala will abolish such specific interactions to stabilize AsA, causing a prompt release of the proton from the bound AsA, leading to a faster electron transfer from the AsA to the heme iron. Further, conversion to the more hydrophobic environments upon the substitution of Tyr⁷¹ with Ala would destabilize a negatively-charged AsA in its binding site. This interpretation might be supported by the observation that Y71A-H₆ mutant showed a very similar property with that of R72A-H₆ mutant. Substitution of Tyr⁷¹ with a more hydrophobic Phe would enhance such a promoting effect by changing the nature of the AsA-binding pocket, which was verified in our present study. The significant lowering of the midpoint potential of the lower potential heme of Y71F-H₆ mutant (Table 1) might be a direct effect of such changes.

More convincing evidence was obtained from the stopped-flow studies on the K83A/Y71A double mutant. The significant lowering of electron accepting ability from AsA at pH 5.0 caused by the K83A mutation (29) (Fig. 4Ba) was rescued by the introduction of a second mutation of Y71A (Fig. 4Bb). However, it is noteworthy that the original pH-dependency observed for WT-Zmb₅₆₁-H₆ (Fig. 4Aa) [which was further enhanced for K83A mutant (29)] was completely lost for its compensation. The resulting behavior of K83A/Y71A double mutant was very similar to that of Y71A-H₆ mutant both in the stopped-flow analysis (Fig. 4Ae) and in the redox potential measurement (Table 1).

From all these pieces of evidence, we propose that both Arg⁷² and Tyr⁷¹ have similar physiological roles for expelling MDA radical from the AsA-binding site (by stabilizing AsA molecule) to prevent a back-flow of electron equivalents from the reduced heme center on the cytosolic side (Fig. 5). Accordingly, both Arg⁷² and Tyr⁷¹ could be classified as group D rather than group B.

It has been shown that electron transfer across the adrenal CG membranes can create a membrane potential (51). Similar energetic considerations on the plant tonoplast would argue that the membrane potential might also affect the rate of transmembrane electron transfer as well. The proton gradient (inside-positive) across the membranes (membrane potential included) is supposed to favor the electron transfer in inward direction both in adrenal CG membranes (52) and in tonoplast membranes. However, in a certain case where the proton gradient was dissipated by acidification of cytosol, the electron equivalents accommodated in the intravesicular AsA would be released by the outward transmembrane electron flow *via* cytochrome b_{561} . In this sense, the mechanistic role of the conserved Arg⁷² and Tyr⁷¹ integrated in cytochrome b_{561} proteins might be very intriguing as a very suitable pH-sensitive switch. To verify our present proposal, however, a detailed structural data based on the X-ray crystallographic study might be highly necessary.

Supplementary material related to this article can be found at <http://dx.doi.org/10.1016/j.jbiosc.2012.11.013>.

ACKNOWLEDGMENTS

This work was supported by Grants-in-Aid for Scientific Research on Priority Areas (System Cell Engineering by Multi-scale Manipulation; 18048030 and 20034034 to M. T.) from the Japanese Ministry of Education, Culture, Sports, Science and Technology and by Grant-in-Aid for Scientific Research (C) (22570142) from Japan Society for the Promotion of Science.

References

1. Trost, P., Bèrczi, A., Sparla, F., Sponza, G., Marzadori, B., Asard, H., and Pupillo, P.: Purification of cytochrome b_{561} from bean hypocotyls plasma

- membrane. Evidence for the presence of two heme centers, *Biochim. Biophys. Acta*, **1468**, 1–5 (2000).
2. **Bérczi, A., Lütjhe, S., and Asard, H.:** *b*-type cytochromes in plasma membranes of *Phaseolus vulgaris* hypocotyls, *Arabidopsis thaliana* leaves, and *Zea mays* roots, *Protoplasma*, **217**, 50–55 (2001).
 3. **Asard, H., Kapila, J., Verelst, W., and Bérczi, A.:** Higher-plant plasma membrane cytochrome *b*₅₆₁: a protein in search of a function, *Protoplasma*, **217**, 77–93 (2001).
 4. **Preger, V., Pesaresi, A., Pupillo, P., and Trost, P.:** Ascorbate-independent electron transfer between cytochrome *b*₅₆₁ and a 27 kDa ascorbate peroxidase of bean hypocotyls, *Protoplasma*, **217**, 137–145 (2001).
 5. **Kent, U. M. and Fleming, P. J.:** Purified cytochrome *b*₅₆₁ catalyzes transmembrane electron transfer for dopamine β-hydroxylase and peptidyl glycine α-amidating monooxygenase activities in reconstituted systems, *J. Biol. Chem.*, **262**, 8174–8178 (1987).
 6. **Perin, M. S., Fried, V. A., Slaughter, C. A., and Südhof, T. C.:** The structure of cytochrome *b*₅₆₁, a secretory vesicle-specific electron transport protein, *EMBO J.*, **7**, 2697–2703 (1988).
 7. **Tsubaki, M., Nakayama, M., Okuyama, E., Ichikawa, Y., and Hori, H.:** Existence of two heme B centers in cytochrome *b*₅₆₁ from bovine adrenal chromaffin vesicles as revealed by a new purification procedure and EPR spectroscopy, *J. Biol. Chem.*, **272**, 23206–23210 (1997).
 8. **Asard, H., Terol-Alcayde, J., Preger, V., Del Favero, J., Verelst, W., Sparla, F., Pérez-Alonso, M., and Trost, P.:** *Arabidopsis thaliana* sequence analysis confirms the presence of cyt *b*-561 in plants: evidence for a novel protein family, *Plant Physiol. Biochem.*, **38**, 905–912 (2000).
 9. **Mckie, A. T., Barrow, D., Latunde-Dada, G. O., Rolfs, A., Sager, G., Mudaly, E., Mudaly, M., Richardson, C., Barlow, D., Bomford, A., and other 6 authors:** An iron-regulated ferric reductase associated with the absorption of dietary iron, *Science*, **291**, 1755–1759 (2001).
 10. **Zhang, D.-L., Su, D., Bérczi, A., Vargas, A., and Asard, H.:** An ascorbate-reducible cytochrome *b*₅₆₁ is localized in macrophage lysosomes, *Biochim. Biophys. Acta*, **1760**, 1903–1913 (2006).
 11. **Bérczi, A. and Asard, H.:** Expression and purification of the recombinant mouse tumor suppressor cytochrome *b*₅₆₁ protein, *Acta Biol. Szeged.*, **52**, 257–265 (2008).
 12. **Recuenco, M. C., Fujito, M., Rahman, M. M., Sakamoto, Y., Takeuchi, F., and Tsubaki, M.:** Functional expression and characterization of human *101F6* protein, a homologue of cytochrome *b*₅₆₁ and a candidate tumor suppressor gene product, *BioFactors*, **34**, 219–230 (2009).
 13. **Tsubaki, M., Takeuchi, F., and Nakanishi, N.:** Cytochrome *b*₅₆₁ protein family: expanding roles and versatile transmembrane electron transfer abilities as predicted by a new classification system and protein sequence motif analyses, *Biochim. Biophys. Acta*, **1753**, 174–190 (2005).
 14. **Okuyama, E., Yamamoto, R., Ichikawa, Y., and Tsubaki, M.:** Structural basis for the electron transfer across the chromaffin vesicle membranes catalyzed by cytochrome *b*₅₆₁: analyses of cDNA nucleotide sequences and visible absorption spectra, *Biochim. Biophys. Acta*, **1383**, 269–278 (1998).
 15. **Tsubaki, M., Kobayashi, K., Ichise, T., Takeuchi, F., and Tagawa, S.:** Diethyl pyrocarbonate-modification abolishes fast electron accepting ability of cytochrome *b*₅₆₁ from ascorbate but does not influence on electron donation to monodehydroascorbate radical: distinct roles of two heme centers for electron transfer across the chromaffin vesicle membranes, *Biochemistry*, **39**, 3276–3284 (2000).
 16. **Takeuchi, F., Kobayashi, K., Tagawa, S., and Tsubaki, M.:** Ascorbate inhibits the carbethoxylation of two histidyl and one tyrosyl residues indispensable for the transmembrane electron transfer reaction of cytochrome *b*₅₆₁, *Biochemistry*, **40**, 4067–4076 (2001).
 17. **Takigami, T., Takeuchi, F., Nakagawa, M., Hase, T., and Tsubaki, M.:** Stopped-flow analyses on the reaction of ascorbate with cytochrome *b*₅₆₁ purified from bovine chromaffin vesicle membranes, *Biochemistry*, **42**, 8110–8118 (2003).
 18. **Kobayashi, K., Tsubaki, M., and Tagawa, S.:** Distinct roles of two heme centers for transmembrane electron transfer in cytochrome *b*₅₆₁ from bovine adrenal chromaffin vesicles as revealed by pulse radiolysis, *J. Biol. Chem.*, **273**, 16038–16042 (1998).
 19. **Asard, H., Venken, M., Caubergs, R., Reijnders, W., Oltmann, F. L., and De Greef, J. A.:** *b*-Type cytochromes in higher plant plasma membranes, *Plant Physiol.*, **90**, 1077–1083 (1989).
 20. **Griesen, D., Su, D., Bérczi, A., and Asard, H.:** Localization of an ascorbate-reducible cytochrome *b*₅₆₁ in the plant tonoplast, *Plant Physiol.*, **134**, 726–734 (2004).
 21. **Nanasato, Y., Akashi, K., and Yokota, A.:** Co-expression of cytochrome *b*₅₆₁ and ascorbate oxidase in leaves of wild watermelon under drought and high light conditions, *Plant Cell Physiol.*, **46**, 1515–1524 (2005).
 22. **Bérczi, A., Su, D., and Asard, H.:** An *Arabidopsis* cytochrome *b*₅₆₁ with transmembrane ferrireductase capability, *FEBS Lett.*, **581**, 1505–1508 (2007).
 23. **Njus, D. and Kelley, P. M.:** The secretory-vesicle ascorbate-regenerating system: a chain of concerted H⁺/e⁻-transfer reactions, *Biochim. Biophys. Acta*, **1144**, 235–248 (1993).
 24. **Vargas, J. D., Hershers, B., Mckie, A. T., Gledhill, S., McDonnell, J., van der Heuvel, M., Davies, K. E., and Ponting, C. P.:** Stromal cell-derived receptor 2 and cytochrome *b*₅₆₁ are functional ferric reductase, *Biochim. Biophys. Acta*, **1651**, 116–123 (2003).
 25. **Su, D. and Asard, H.:** Three mammalian cytochrome *b*₅₆₁ are ascorbate-dependent ferrireductases, *FEBS J.*, **273**, 3722–3734 (2006).
 26. **Bérczi, A., Caubergs, R. J., and Asard, H.:** Partial purification and characterization of an ascorbate-reducible *b*-type cytochrome from the plasma membrane of *Arabidopsis thaliana* leaves, *Protoplasma*, **221**, 47–56 (2003).
 27. **Verelst, W., Kapila, J., de Almeida Engler, J., Stone, J. M., Caubergs, R. J., and Asard, H.:** Tissue-specific expression and developmental regulation of cytochrome *b*₅₆₁ genes in *Arabidopsis thaliana* and *Raphanus sativus*, *Physiol. Plant.*, **120**, 312–318 (2004).
 28. **Rahman, M. M., Nakanishi, N., Takigami, T., Hase, T., Park, S.-Y., and Tsubaki, M.:** Purification and biochemical analysis of *Zea mays* cytochrome *b*₅₆₁ heterologously expressed in *Pichia pastoris*, pp. 108–112, in: MHS2007. International Symposium on Micro-NanoMechatronics and Human Science, 2007. IEEE, Nagoya (2007).
 29. **Nakanishi, N., Rahman, M. M., Sakamoto, Y., Takigami, T., Kobayashi, K., Hori, H., Hase, T., Park, S.-Y., and Tsubaki, M.:** Importance of conserved Lys83 residue of *Zea mays* cytochrome *b*₅₆₁ for ascorbate-specific transmembrane electron transfer as revealed by site-directed mutagenesis studies, *Biochemistry*, **48**, 10665–10678 (2009).
 30. **Nakanishi, N., Takeuchi, F., and Tsubaki, M.:** Histidine cycle mechanism for the concerted proton/electron transfer from ascorbate to the cytosolic heme *b* center of cytochrome *b*₅₆₁: a unique machinery for the biological transmembrane electron transfer, *J. Biochem.*, **142**, 553–560 (2007).
 31. **Nakanishi, N., Rahman, M. M., Sakamoto, Y., Miura, M., Takeuchi, F., Park, S.-Y., and Tsubaki, M.:** Inhibition of electron acceptance from ascorbate by the specific *N*-carbethoxylations of maize cytochrome *b*₅₆₁: a common mechanism for the transmembrane electron transfer in cytochrome *b*₅₆₁ protein family, *J. Biochem.*, **146**, 857–866 (2009).
 32. **Bérczi, A., Su, D., Lakshminarasimhan, M., Vargas, A., and Asard, H.:** Heterologous expression and site-directed mutagenesis of an ascorbate-reducible cytochrome *b*₅₆₁, *Arch. Biochem. Biophys.*, **443**, 82–92 (2005).
 33. **Lakshminarasimhan, M., Bérczi, A., and Asard, H.:** Substrate-dependent reduction of a recombinant chromaffin granule Cyt-*b*₅₆₁ and its R72A mutant, *Acta Biol. Szeged.*, **50**, 61–65 (2006).
 34. **Bérczi, A. and Asard, H.:** Characterization of an ascorbate-reducible cytochrome *b*₅₆₁ by site-directed mutagenesis, *Acta Biol. Szeged.*, **50**, 55–59 (2006).
 35. **Laemmli, U. K.:** Cleavage of structural proteins during the assembly of the head of bacteriophage T₄, *Nature*, **227**, 680–685 (1970).
 36. **Dutton, P. L.:** Redox potentiometry: determination of midpoint potentials of oxidation-reduction components of biological electron-transfer systems, *Methods Enzymol.*, **54**, 411–435 (1978).
 37. **Walker, F. A., Huynh, B. H., Scheidt, W. R., and Osvath, S. R.:** Models of the cytochromes *b*. Effect of axial ligand plane orientation on the EPR and Mössbauer spectra of low-spin ferrihemes, *J. Am. Chem. Soc.*, **108**, 5288–5297 (1986).
 38. **Williams, N. H. and Yandell, J. K.:** Outer-sphere electron-transfer reactions of ascorbate anions, *Aust. J. Chem.*, **35**, 1133–1144 (1982).
 39. **Laroff, G. P., Fessenden, R. W., and Schuler, R. H.:** The electron spin resonance spectra of radical intermediates in the oxidation of ascorbic acid and related substances, *J. Am. Chem. Soc.*, **94**, 9062–9073 (1972).
 40. **Rahman, M. M., Nakanishi, N., Fujito, M., Miura, M., Hase, T., Park, S.-Y., Hori, H., and Tsubaki, M.:** Inhibition of the electron transfer of plant cytochrome *b*₅₆₁ by the modification with diethylpyrocarbonate: in search of a common mechanism for the transmembrane electron transfer from ascorbate, pp. 157–162, in: MHS2008. International Symposium on Micro-NanoMechatronics and Human Science, 2008. IEEE, Nagoya (2008).
 41. **Sharp, K. H., Mewies, M., Moody, P. C. E., and Raven, E. L.:** Crystal structure of the ascorbate peroxidase-ascorbate complex, *Nat. Struct. Biol.*, **10**, 303–307 (2003).
 42. **Li, S., Taylor, K. B., Kelly, S. J., and Jędrzejak, M. J.:** Vitamin C inhibits the enzymatic activity of *Streptococcus pneumoniae* hyaluronate lyase, *J. Biol. Chem.*, **276**, 15125–15130 (2001).
 43. **Burmeister, W. P., Cottaz, S., Rollin, P., Vasella, A., and Henrissat, B.:** High resolution X-ray crystallography shows that ascorbate is a cofactor for myrosinase and substrates for the function of the catalytic base, *J. Biol. Chem.*, **275**, 39385–39393 (2000).
 44. **Linley, P. J., Landsberger, M., Kohchi, T., Cooper, J. B., and Terry, M. J.:** The molecular basis of heme oxygenase deficiency in the *pcd1* mutant of pea, *FEBS J.*, **273**, 2594–2606 (2006).
 45. **Murphy, E. J., Metcalfe, C. L., Basran, J., Moody, P. C. E., and Raven, E. L.:** Engineering the substrate specificity and reactivity of a heme protein: creation of an ascorbate binding site in cytochrome *c* peroxidase, *Biochemistry*, **47**, 13933–13941 (2008).
 46. **Ludwiczek, S., Rosell, F. I., Ludwiczek, M. L., and Maul, A. G.:** Recombinant expression and initial characterization of the putative human enteric ferric reductase Dcytb, *Biochemistry*, **47**, 753–761 (2008).